Lattice description of electron loss in high-energy $H^+ + H_2O$ collisions.

L. F. Errea, Clara Illescas, L. Méndez, I. Rabadán, J. Suárez

Laboratorio Asociado al CIEMAT de Física Atómica y Molecular en Plasmas de Fusión. Departamento de Química, Módulo 13, Universidad Autónoma de Madrid, 28049 Madrid, Spain

Abstract

Electron loss in proton-water collisions is studied in the energy range 100 keV $< E <$ 1 MeV by employing a three-center model potential. The electron-loss probabilities are calculated by applying a new lattice method that yields cross sections which are in good agreement with previous semi-classical close-coupling and classical calculations. The lattice method also provides a straightforward visualization of the ionization mechanism at high impact velocities that involves a quasi-free expansion of the electron cloud.

Keywords: Lattice methods. Ion-molecule scattering. Ionization.
PACS: 34.50.Gb, 34.50.-s, 34.70.+e

1. Introduction

Ionization of water molecules by ion impact is an important process in radiation damage of biological systems because the low-energy electrons released in these reactions cause DNA strand breaking [1]. Furthermore, the water cations produced in those reactions dissociate, giving rise to several ions and radicals which also cause DNA breaking. On the other hand, ion-water collisions take place in cometary and planetary atmospheres, where electron capture reactions by solar wind ions are responsible for X-ray and UV emission [2].

Ion-water collisions may lead to electron capture reactions:

$$X^{q+} + H_2O \rightarrow X^{(q-p)+} + H_2O^{p+} \tag{1}$$

Email address: l.mendez@uam.es (L. F. Errea, Clara Illescas, L. Méndez, I. Rabadán, J. Suárez)

and ionization processes:

$$X^{q+} + H_2O \rightarrow X^{q+} + H_2O^{r+} + re^- \,. \tag{2}$$

Transfer-ionization processes of the form

$$X^{q+} + H_2O \rightarrow X^{(q-p)+} + H_2O^{(p+r)+} + re^- \,, \tag{3}$$

are also possible, where target electrons are removed in simultaneous capture and ionization reactions. Experiments often provide cross sections for electron production, which refers to the total number of electron released in ionization and transfer-ionization. For the particular case of proton-H_2O collisions, the two-electron capture process is unlikely to happen, and, therefore, $p = 1$ in Eqs. (1) and (3).

Previous calculations on ionization in ion - H_2O collisions generally employ the independent electron approximation that assumes that the active electron moves in the average field created by the nuclei and the other electrons. In particular, electron capture and ionization cross sections have been calculated by applying the first Born approximation [3], the continuum-distorted-wave method [4, 5, 6, 7, 8, 9, 10], the classical trajectory Monte Carlo (CTMC) [11, 12, 13, 14] and the semiclassical treatment with pseudostates [15, 16, 17, 18]. The one-electron probabilities yielded by these calculations are then combined (see [19, 20]) to obtain the probabilities for the many-electron processes. For instance, the electron production probability $P^{\rm EP}$, in ion collisions with H_2O is given by the simple relationship [21]:

$$P^{\rm EP} = \sum_{\alpha} \alpha p_{\alpha} = 2 \sum_{k=1}^{N_{\rm occ}} p_k^{\rm I} \,. \tag{4}$$

where p_α is the probability of releasing α electrons to the continuun, and $p_k^{\rm I}$ is the calculated one-electron ionization probability of an electron occupying initially the k-th molecular orbital (MO) of the target and $N_{\rm occ}$ is the number of doubly occupied MOs. For collisions with the water molecule, $N_{\rm occ}$ can be taken equal to four (the number of valence MOs), except at very high collision energies, where core electrons are also released.

Within the framework of the independent particle model, the discrepancies found in the electron production probabilities reported so far arise from differences in the evaluation of the one-electron probabilities. In this respect, the aim of the present work is to gauge the usefulness of a method based on the numerical solution of the time-dependent Schrödinger equation (TDSE), comparing the results with those of ref. [13], which lead to

electron-loss total cross sections in good agreement with the experimental data at collision energies above 25 keV/u [22, 23, 24].

Previous works [25, 26, 27, 28] have employed lattice methods to study electron capture in ion-atom collisions. Wave packet propagation techniques [29, 30, 31, 32] have been also employed to solve the radial equations in low-energy ion-atom collisions. To our knowledge, lattice methods have not been applied to ion-molecule collisions. Our treatment is based on the GridTDSE [33] parallel computational package that we have recently applied to study the predissociation of the water cation [34]. In addition to the calculation of electron transition probabilities, the numerical integration of the TDSE provides a direct visualization of the electronic dynamics.

The paper is organized as follows: In section 2 we present the lattice method employed to solve numerically the TDSE. the results of the numerical calculations are shown and compared to those of Ref. [13] in section 3. A brief summary is presented in section 4. Atomic units are employed unless otherwise stated.

2. Computational methods

In the high velocity range considered in this work, we can assume that the projectile follows rectilinear trajectories with impact parameter $\boldsymbol{b}$ and velocity $\boldsymbol{v}$.a We have also employed the Franck-Condon approximation, in which the target nuclei remain at their equilibrium positions during the collision. Previous calculations on ion-diatom collisions ([35] and references therein) indicates that the approximation is valid for energies above 1 keV/u. In order to describe the electron-target interaction, we have used a three-center model potential:

$$V_{\rm mod}(\boldsymbol{r}) = V_{\rm O}(r_{\rm O}) + V_{\rm H}(r_{\rm H_1}) + V_{\rm H}(r_{\rm H_2}) \tag{5}$$

where $r_{\rm O}, r_{\rm H_1}$ and $r_{\rm H_2}$ are the electron distances to the three water nuclei O, H_1 and H_2, respectively. The three terms in (5) are parameterized according to the expressions:

$$V_{\rm O}(r_{\rm O}) = -\frac{8-N_{\rm O}}{r_{\rm O}} - \frac{N_{\rm O}}{r_{\rm O}}\left(1+\alpha_{\rm O} r_{\rm O}\right)\exp(-2\alpha_{\rm O} r_{\rm O}) \tag{6}$$

$$V_{\rm H}(r_{\rm H_{1,2}}) = -\frac{1-N_{\rm H}}{r_{\rm H_{1,2}}} - \frac{N_{\rm H}}{r_{\rm H_{1,2}}}\left(1+\alpha_{\rm H} r_{\rm H_{1,2}}\right)\exp(-2\alpha_{\rm H} r_{\rm H_{1,2}})\,, \tag{7}$$

where $N_{\rm H} = (9-N_{\rm O})/2$, and the parameters $\alpha_{\rm H}$, $\alpha_{\rm O}$ and $N_{\rm O}$ are optimized with the criterion of minimizing the differences between the eigenvalues ϵ_k of

the one-electron Hamiltonian $-\frac{1}{2}\nabla^2 + V_{\rm mod}$ and the SCF energies. In practice, we have employed $\alpha_{\rm H} = 0.617 a_0^{-1}$, $\alpha_{\rm O} = 1.6025 a_0^{-1}$ and $N_{\rm O} = 7.185$ for the three highest occupied MOs ($1b_2$, $3a_1$ y $1b_1$).

In the impact parameter treatment, the electronic wave function $\Phi^k(\boldsymbol{r}, t)$ is a solution of the semiclassical equation:

$$\left[h_{\rm el}^{\rm MP} - {\rm i} \left. \frac{\partial}{\partial t} \right|_r \right] \Phi^k = 0, \tag{8}$$

which is formally identical to the TDSE. Eq. 8 is solved with the initial condition

$$\Phi^k \underset{t \to -\infty}{\sim} \phi^k \exp(-{\rm i}\epsilon_k t) \tag{9}$$

where

$$h_{\rm el}^{\rm MP} = -\frac{1}{2}\nabla^2 + V_{\rm mod} - \frac{Z_{\rm P}}{r_{\rm P}} = h_{\rm T} - \frac{Z_{\rm P}}{r_{\rm P}}. \tag{10}$$

ϕ^k is the initial MO, which is an eigenfunction of $h_{\rm T}$, and the origin of the electronic coordinates is placed on the center of mass of the molecule.

In the present work, we have employed the program GridTDSE [33] to reproduce the evolution of the electronic wave function in a 3D Cartesian coordinate grid. The program was originally written for calculating the time evolution of a nuclear wave packet on a single potential energy surface, and we have extended the application to solve the electronic wave equation on time-dependent fields. If one places the electron coordinates origin on the target center of mass, the solution of this equation is initially a MO of the water molecule [see Eq. (9)], which is evaluated on the grid points to yield the vector $\boldsymbol{\phi^k}$. The potential energy operator is expressed as a diagonal matrix at each grid point, while the electronic kinetic energy operator is obtained by applying finite difference algorithms that render a multi-diagonal sparse $\boldsymbol{h}_{\rm el}^{\rm MP}$ matrix (see [36]).

The description of the initial wavefunctions in the lattice calculation has been checked by comparing the energies of the MOs, calculated with a Lanczos propagation scheme, with those obtained by solving the secular equation for $h_{\rm T}$ in the the basis of Gaussian-Type-Orbitals (GTO) of reference [13] and the same model potential . In Table 1 we show this comparison for the three highest occupied MOs with two grid densities (G10: 10 points/a_0 on each direction; G25: 25 points/a_0 on each direction).

We have used the second-order differences method to solve Eq. (8) to obtain the wave function at different times:

$$\boldsymbol{\Phi}^k(t + \Delta) = \boldsymbol{\Phi^k}(t - \Delta) - 2{\rm i}\Delta \boldsymbol{h}_{\rm el}^{\rm MP} \boldsymbol{\Phi}^k(t). \tag{11}$$

Orbital	G10	G25	GTO
$1b_1$	-0.523	-0.518	-0.519
3a1	-0.543	-0.568	-0.578
$1b_2$	-0.739	-0.737	-0.737

Table 1: Comparison of the energies of the MOs of H_2O calculated using a GTO basis and the lattice method with two grid densities (see text).

Φ^k is propagated from t_i to t_f in a uniform Cartesian grid of about 33×10^6 points with the electronic coordinates in the interval $-16\ \mathrm{a}_0 \leq q_i \leq 16\ \mathrm{a}_0$ and $r_{i+1} - q_i = 0.1\ \mathrm{a}_0$ ($q = x, y, z$). This grid size requires a memory allocation of ~ 50 Gb. We have checked that the transition probabilities do not change when the grid is limited to the interval $[-12, 12]$, keeping the same density.

In order to avoid nonphysical reflections in the grid walls, we have included in the propagation scheme a mask function of the form [37]:

$$M(\boldsymbol{r}) = \prod_{i=1,3} \begin{cases} 1 & \text{if} \quad q_i^{L-} < q_i < q_i^{L+} \\ \exp\left\{-\sigma_i (q_i - q_i^{L\pm})^2\right\} & \text{elsewhere} \end{cases} \tag{12}$$

with $\sigma_i = 0.01\ \mathrm{a}_0^{-2}$ and $q_i^{L\pm} = \pm 15\ \mathrm{a}_0$; this mask function leads to a smooth decay of the wave packet for $q_i \gtrsim 15\ a_0$.

The norm of the wave packet after the collision represents the probability that the electron remains bound to the target molecule:

$$p_\mathrm{T}^k = \lim_{t\to t_\mathrm{f}} \|\boldsymbol{\Phi}^k\|^2 \ ; \tag{13}$$

i.e., the probability for elastic scattering or electronic excitation, and

$$p_\mathrm{EL}^k = \lim_{t\to t_\mathrm{f}} \left[1 - \|\boldsymbol{\Phi}^k\|^2\right] \tag{14}$$

is the electron-loss (EL) probability, which is the sum of ionization and electron capture probabilities. As the energy increases, the electron capture probability decreases, and p_EL^k becomes equal to the ionization probability.

In model potential calculations, there is a non vanishing probability of populating occupied MOs of the target, $\phi^l, l \neq k$, eigenfunctions of h_T. This unphysical situation is avoided to some extent in close-coupling calculations

by decoupling the channels dissociating into occupied MOs from the other channels. In this work, we have implemented an alternative based on the use of a Phillips-Kleinman (PK) pseudopotential [38]; explicitly, the electronic Hamiltonian has the form:

$$h_{\rm el}^{\rm PK} = -\frac{1}{2}\nabla^2 + V_{\rm mod} - \frac{Z_{\rm P}}{r_{\rm P}} + M \sum_{l=1,l\neq k}^{N_{\rm occ}} |\phi^l >< \phi^l| \,, \tag{15}$$

where M is a large arbitrary constant ($M \approx 100$ Hartree), which prevents transitions to the occupied orbitals during the collision. The lattice calculation is therefore modified by adding the term:

$$\boldsymbol{V}^{\rm PK} = M \sum_{l=1,l\neq k}^{N_{\rm occ}} \boldsymbol{\phi^l}\boldsymbol{\phi^l}^{\dagger} \tag{16}$$

to the Hamiltonian matrix, where $\boldsymbol{\phi^l}$ are the column eigenvectors of the matrix $\boldsymbol{h}_{\rm T}$.

We have evaluated orientation-averaged transition probabilities using the 12 trajectory orientations described in Ref. [12] (see Fig. 1). These orientations are defined with respect to a fixed reference frame where the H_2O nuclei are in the plane XZ and the C_2 axis lies along the Z direction. In some illustrations we shall consider a particular trajectory, t_4 of Fig. 1, with $\boldsymbol{b} \parallel \widehat{X}$ and $\boldsymbol{v} \parallel \widehat{Y}$, that yields probabilities similar to the orientation-averaged ones in the CTMC calculations.

3. Results

In this section we present the results for EL in proton collisions with H_2O molecules. The results are illustrated for collisions where the active electron is initially described by the $1b_1$ and $1b_2$ orbitals of H_2O. The choice of these two orbitals is not arbitrary since they play different roles in the chemical bonding. $1b_1$ is the HOMO orbital, essentially a non-bonding $2p_y$ orbital of the oxygen atom, perpendicular to the molecular plane, while the electron occupying the $1b_2$ orbital is delocalized between the oxygen and hydrogen atoms, and its removal leads to the formation of $H_2O^+(\tilde{B}\ ^2B_2)$, which readily predissociates following the mechanism recently described in Ref. [34].

The first goal of our calculations is to gauge the importance of using a PK pseudopotential term in the system hamiltonian to avoid electron flux from one valence MO of H_2O to the rest of them. This is illustrated in Fig. 2 by comparing with results without the PK term. The calculations

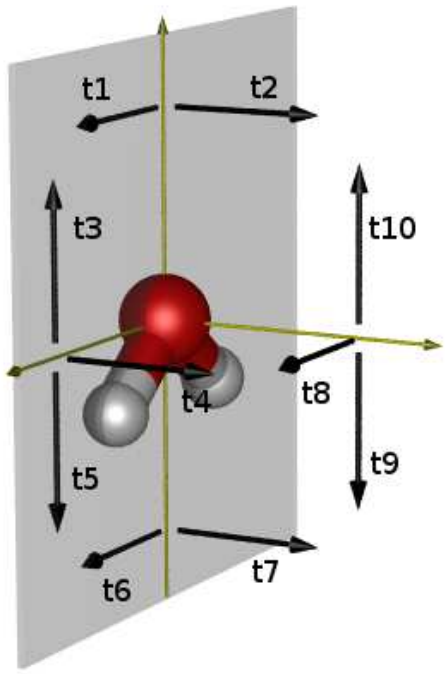

Figure 1: Trajectory orientations employed in the orientation average procedure.

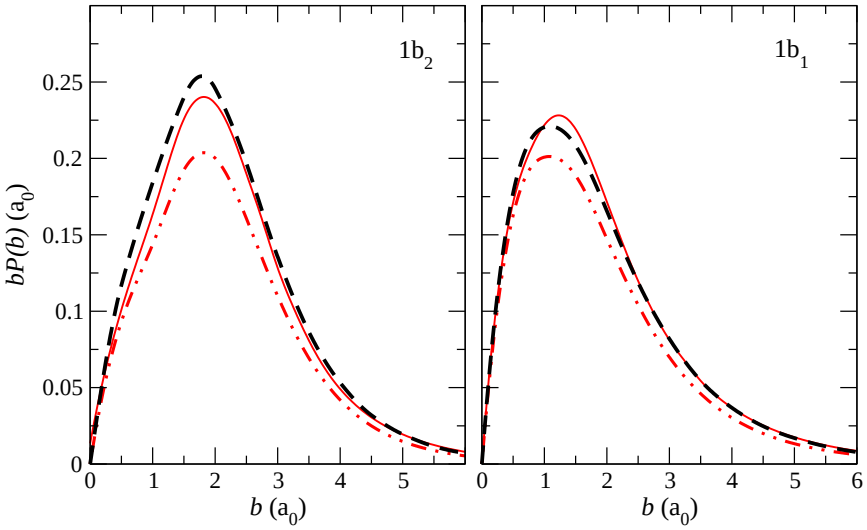

Figure 2: Electron-loss opacities, $bP^k_{\rm EL}(b)$, as functions of b in proton collisions with H_2O at $E = 100$ keV and with the electron initially on MOs $1b_1$ and $1b_2$ (indicated in the panels) for the t_4 trajectory, as indicated in the text. Solid lines are the results including the PK pseudopotential in the Hamiltonian [Eq. (15)], and the dotted-dashed are those without the PK pseudopotential. The dashed lines correspond to the semiclassical AFMO results.

have been performed for the representative trajectory t_4, considering the electron initially located in the MOs $1b_1$ and $1b_2$. One can note, for both MOs, that the EL probabilities increase when the PK term is added, because the nonphysical trapping of the electronic flux is removed.

The reliability of the lattice method is tested in Fig. 2 by comparing the EL probabilities with those obtained by means of the semiclassical close-coupling method of Refs. [13, 39], which also relies in the use of a fitted pseudopotential and the same orientation-average procedure to obtain ionization and electron-loss cross sections. In those calculations, carried out with asymptotic-frozen molecular orbitals (AFMO), the couplings between the doubly occupied MOs were taken equal to zero. A very good agreement is found between the AFMO and the lattice results, with the PK term included in the latter. On the other hand, we have checked that the EL probabilities for trajectory t_4 change in less than 0.5% when the box is extended from 16 to 17 a_0 on each direction, which permits that the absorption by the mask function (12) takes place from 15 to 17 a_0; this indicates that the reflection in the box walls is not relevant.

We analyze in Fig. 3 the convergence of the lattice calculation with respect to the final integration time t_f by plotting the EL probability as a function of vt for trajectories with $b = 1.5$ a_0. This figure shows that the electron-loss process starts near the point of closest approach ($t = 0$) between the projectile and the target, and it is followed by a smooth decay of the norm. Previous calculations have shown that electron capture is a small fraction ($\approx 10\%$) of the EL probability, which allows us to interpret the shape of this curves as a consequence of the ionization mechanisms that involve a direct proton-electron interaction, followed by a slow diffusion of the ionizing cloud (see [40]). The slow decrease of the electron-loss probability above $vt \sim 150$ a_0 reflects the slow expansion of part of the wave function, which points to the emission of low-energy electrons, in line with the differential cross sections of Ref. [12]. In the lattice treatment, the EL probability is calculated as the fraction of the electronic wave packet that leaves the box where the grid is defined, and the slowest components of the electron wave packet need a sizeable time to reach the box borders. Furthermore, the fact that none of the three curves in Fig. 3 have converged at $vt = 100$ a.u. is a consequence of the above mentioned free expansion of the ionizing cloud, which is independent of the projectile velocity in the energy range considered.

The mechanism of the EL reaction is further illustrated in Fig. 4, where we show snapshots of the evolution of $|\mathbf{\Phi}^k|^2$ (with $k \equiv 1b_1$, $1b_2$) at four values of t. The range adopted in the density scale is intentionally low in order to show the evolution of the small part of the wave function which leads to ionization. When the electron is initially on the $1b_1$ MO, we have represented the wavefunction on the plane XY, the proton velocity is parallel to the Y axis and the orbital $1b_1$ is almost identical to the oxygen $2p_y$ orbital. The plots show that for $t < 0$, that is, when the projectile is approaching the target, no sizeable transitions are observed. Significant changes only occur when the projectile steps in the inner part of the molecular orbital. At $t = 2$ a.u., the electronic cloud is partially dragged by the projectile and, simultaneously, a rotation of the cloud takes place, as described in refs. [40, 41] for ion-atom collisions. As t increases, the projectile heads towards the border of the grid, and the part of the electron cloud which is partially captured moves attached to it. A considerable part of the electron cloud has gained enough kinetic energy as to escape from the target. Finally, at $t = 20$ a.u. the projectile has abandoned the box together with part of the electron cloud, which, in our calculation, is accounted for through the absorption by the mask function. Simultaneously, the continuum component of the wavefunction starts to be clear in the plots as nodes along the direction

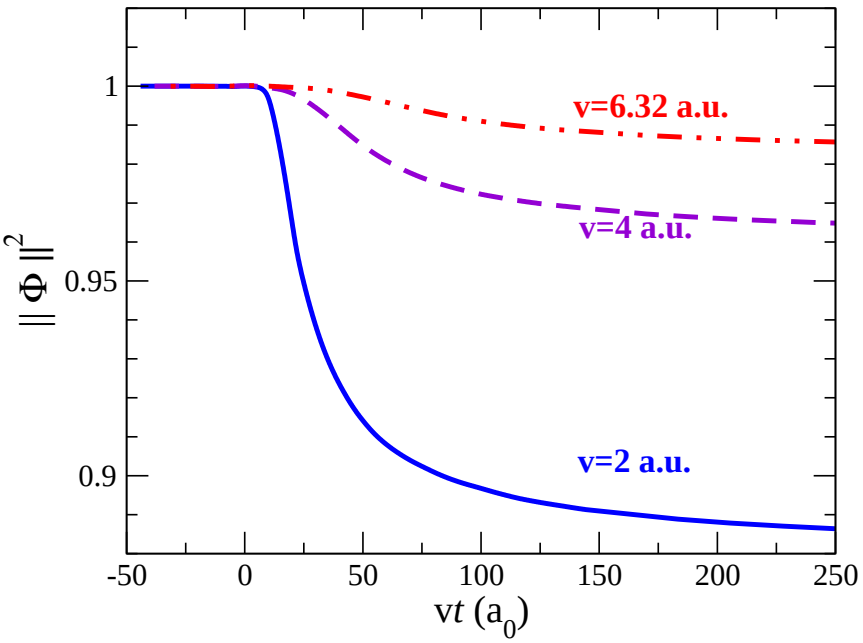

Figure 3: Time evolution of the orientation-averaged $\|\mathbf{\Phi}^k\|^2$ with $k \equiv 1b_1$ for $b = 1.5$ a_0 and three projectile velocities corresponding to impact energies of $E = 100$ ($v = 2$ a.u.), 400 ($v = 4$ a.u.) and 1000 keV ($v = 6.32$ a.u.).

of the Y axis. The ionization mechanism found in our calculation is similar to that described in Ref. [41] for ion-atom collisions: The ionization takes place as a sudden perturbation when the projectile is close to the target, where the electron capture takes place. Part of the electronic cloud is unable to follow the fast projectile motion and leads to ionization. This initial step is followed by a free expansion of the ionizing cloud.

In order to illustrate more clearly the mechanism, we display in the right panels of Fig. 4 the time evolution of the wave function from the $1b_2$ orbital and the same trajectory t_4. In those panels, the density functions are plotted on the molecular plane that is crossed by the proton trajectory at $t = 0$. In this case, the sphere is located at the point of closest approach ($X = b = 1.5$ a$_0$, $Z = 0$). As the projectile moves perpendicularly to the molecular plane, the capture process does not involve a significant expansion of the electron cloud in the plane of representation, and the broadening of the wave function is due to ionization. The mechanism found for EL from the $1b_2$ orbital is quite similar to the one for $1b_1$. As in the previous case, the distribution of the electron cloud is only modified when the projectile reaches the inner part of the orbital. However, in this case the continuum component of the wave function is distinctly more isotropic, and the electron flux is moving in both directions, X and Y.

The comparison between EL probabilities from AFMO and lattice methods is illustrated in Fig. 5, where we consider both the t_4 and the orientation-averaged probabilities. One can note the conspicuous agreement between both sets of results. This is a particularly relevant point given that both calculations employ completely different methods to obtain the collision wavefunction. The EL probabilities decrease as the impact energy increases, consequence of a decreasing interaction time.

4. Summary and Conclusions

In the present work we have implemented a 3D lattice method for solving the electronic wave equation in proton - molecule collisions at high energies ($E > 100$ keV), based on the one-electron approximation. The method uses a model potential to describe the active electron interaction with the molecular core. A Phillips-Kleinman pseudopotential has been included to avoid the electron being "excited" to MOs that are doubly occupied. Previous semiclassical calculations (AFMO) on proton - H_2O collisions were carried out by employing a basis set of GTOs centered on the nuclei, and a large basis that is required to describe the transitions to the electronic continuum. The excellent agreement between the two methods, for each projectile

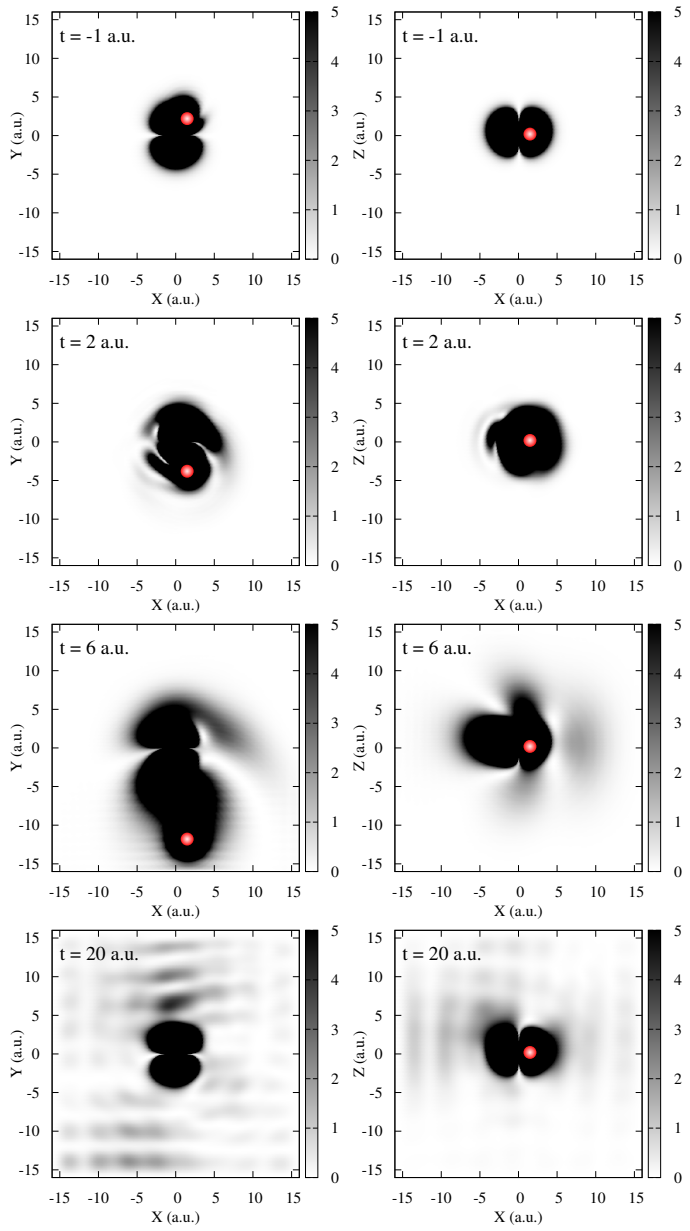

Figure 4: Density plots of $|\mathbf{\Phi}^k|^2$ for $k \equiv 1b_1$ on the XY plane (left panel) and $k \equiv 1b_2$ on the XZ plane (right panels) for the same nuclear trajectory orientation as in Fig. 2 wiht $b = 1.5$ a_0 and $E = 100$ keV. In the panels, the densities are multiplied by 10^5 The snapshots are taken at times indicated in the panels. The sphere indicates the position of the proton (not scaled) along the trajectory. For the sake of clarity, the density color is saturated for values larger than 5×10^{-5} a_0^{-3}.

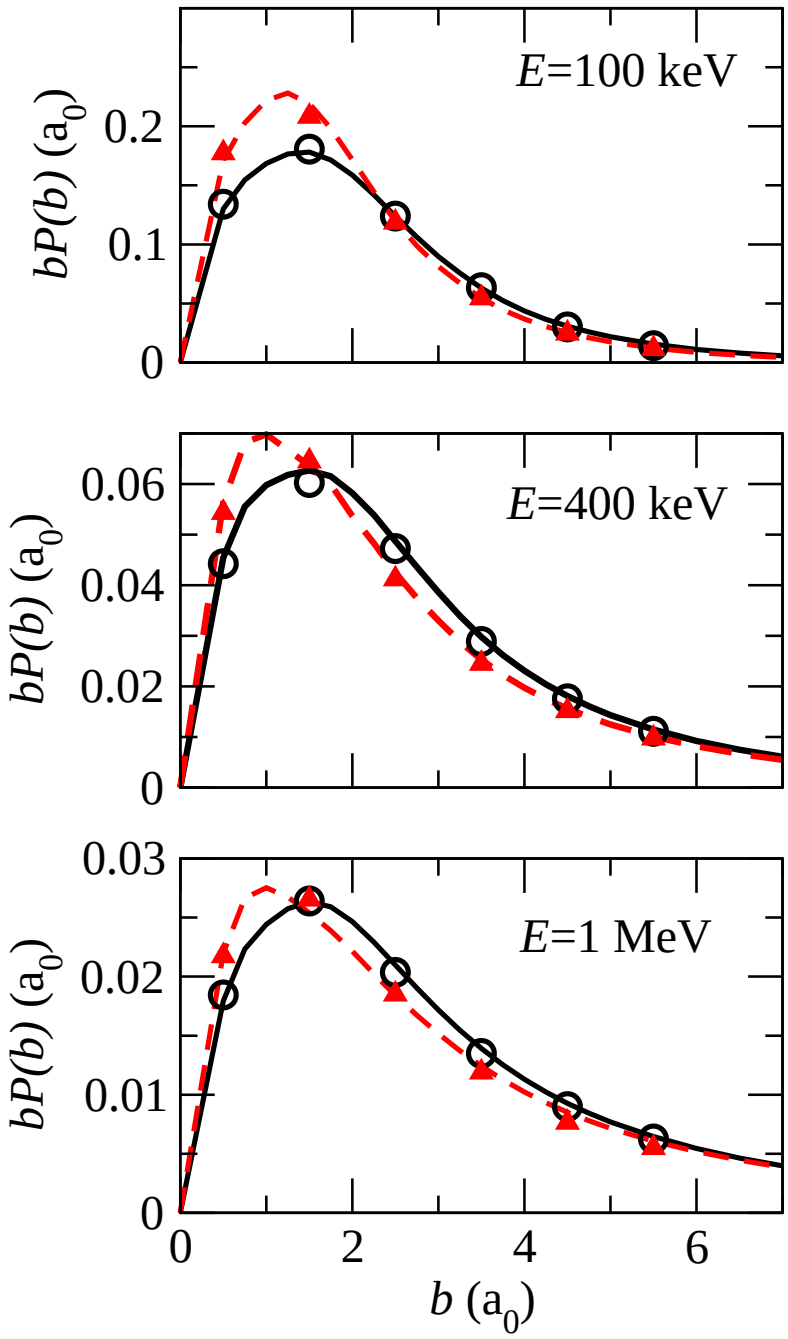

Figure 5: Opacity functions $bP(b)$ for EL from the $1b_1$ MO at three impact energies (indicated in the panels). Dashed and solid lines correspond to the t_4 and orientation-averaged results with the AFMO method, while the solid triangles and open circles are the corresponding lattice results.

trajectory, reinforces the quality of the former semiclassical calculations, in view of the completely different approach taken in both methods. According to this agreement, the lattice grid technique, commonly applied to treat nuclear dynamics problems, has demonstrated an outstanding performance in electron dynamics on the basis of an efficient parallelization procedure.

One of the advantages of the lattice method is its simplicity. Also, it is worth noting that the accuracy of the results can be easily improved by adding grid points to the calculations. The third advantage is that it allows a direct visualization of the electronic cloud as a function of the collision time and, therefore, the collision mechanisms that take place. There are three extensions of the method that can be implemented to treat non-adiabatic transitions in a wide energy range. First, the description of the electron capture reaction can be carried out by performing an additional calculation with the grid centered on the projectile. In this way, the electron capture probability can be evaluated without including electron translation factors, needed in close-coupling calculations. The second extension is the application of the method to evaluate differential cross sections. In particular, the flux of electrons with a given momentum can be obtained by computing the flux of the current at the border of the grid, just before the absorbing region. Finally, the method can be extended to treat collisions with larger molecules, provided that the corresponding model potential is available. Obviously, the numerical calculation of ion collision with larger targets will require the use of larger boxes, with the corresponding increase of the computational resources needed.

5. Acknowledgements

This work has been partially supported by projects ENE2011-28200 and ENE2014-52432-R of the Secretaría de Estado de I+D+i (Spain). Calculations have been performed at the Centro de Computación Científica (UAM, Madrid) and partly at the Barcelona Supercomputing Center (BSC) with financial support from the Red Española de Supercomputación (RES; grants FI-2012-2-0016, FI-2013-1-0020 and FI2013-2-0006).

6. References

[1] B. Boudaïffa, P. Cloutier, D. Hunting, M. A. Huels, L. Sanche, Science 287 (2000) 164.

[2] N. A. Schwadron, T. E. Cravens, The Astrophysical Journal 544 (2000) 558.

[3] O. Boudrioua, C. Champion, C. D. Cappello, Y. V. Popov, Phys. Rev. A 75 (2007) 022720.

[4] P. D. Fainstein, G. H. Olivera, R. D. Rivarola, Nucl. Instr. and Meth. B 107 (1996) 19.

[5] G. H. Olivera, C. Caraby, P. Jardin, A. Cassimi, L. Adoui, B. Gervais, Physics in Medicine and Biology 43 (1998) 2347.

[6] B. Gervais, M. Beuve, G. H. Olivera, M. E. Galassi, Radiat. Phys. Chem. 75 (2006) 493.

[7] C. Champion, O. Boudrioua, C. Dal Cappello, Y. Sato, D. Ohsawa, Phys. Rev. A 75 (2007) 032724.

[8] C. D. Cappello, C. Champion, O. Boudriuoa, H. Lekadir, Y. Sato, D. Ohsawa, Nucl. Instr. and Meth. B. 267 (2009) 781.

[9] A. Dubois, S. Carniato, P. D. Fainstein, J. P. Hansen, Phys. Rev. A 84 (2011) 012708.

[10] C. C. Montanari, J. E. Miraglia, Journal of Physics B: Atomic, Molecular and Optical Physics 47 (2014) 015201.

[11] L. F. Errea, C. Illescas, L. Méndez, B. Pons, I. Rabadán, A. Riera, Phys. Rev. A 76 (2007) 040701.

[12] C. Illescas, L. F. Errea, L. Méndez, B. Pons, I. Rabadán, A. Riera, Phys. Rev. A 83 (2011) 052704.

[13] L. F. Errea, C. Illescas, L. Méndez, I. Rabadán, Phys. Rev. A 87 (2013) 032709.

[14] T. Liamsuwan, H. Nikjoo, Physics in Medicine and Biology 58 (2013) 641.

[15] H. J. Lüdde, T. Spranger, M. Horbatsh, T. Kirchner, Phys. Rev. A 80 (2009) 060702.

[16] M. Murakami, T. Kirchner, M. Horbatsch, H. J. Lüdde, Phys. Rev. A 85 (2012) 052704.

[17] M. Murakami, T. Kirchner, M. Horbatsch, H. J. Lüdde, Phys. Rev. A 85 (2012) 052713.

[18] M. Murakami, T. Kirchner, M. Horbatsch, H. J. Lüdde, Phys. Rev. A 86 (2012) 022719.

[19] J. H. McGuire, L. Weaver, Phys. Rev. A 16 (1977) 41.

[20] L. A. Wehrman, A. L. Ford, J. F. Reading, J. Phys. B: At. Mol. Opt. Phys. 29 (1996) 5831.

[21] T. Kirchner, L. Gulyás, H. J. Lüdde, E. Engel, R. M. Dreizler, Phys. Rev. A 58 (1998) 2063.

[22] M. E. Rudd, T. V. Goffe, R. D. DuBois, L. H. Toburen, Phys. Rev. A 31 (1985) 492–494.

[23] M. A. Bolorizadeh, M. E. Rudd, Phys. Rev. A 33 (1986) 888.

[24] H. Luna, A. L. F. de Barros, J. A. Wyer, S. W. J. Scully, J. Lecointre, P. M. Y. Garcia, G. M. Sigaud, A. C. F. Santos, V. Senthil, M. B. Shah, C. J. Latimer, E. C. Montenegro, Phys. Rev. A 75 (2007) 042711.

[25] M. Chassid, M. Horbatsch, Phys. Rev. A 66 (2002) 012714.

[26] T. Minami, M. S. Pindzola, T.-G. Lee, D. R. Schultz, Journal of Physics B: Atomic, Molecular and Optical Physics 39 (2006) 2877.

[27] T. Minami, T.-G. Lee, M. S. Pindzola, D. R. Schultz, Journal of Physics B: Atomic, Molecular and Optical Physics 41 (2008) 135201.

[28] M. S. Pindzola, D. R. Schultz, Phys. Rev. A 77 (2008) 014701.

[29] N. Vaeck, M.-C. Bacchus-Montabonel, E. Baloïtcha, M. Desouter-Lecomte, Phys. Rev. A 63 (2001) 042704.

[30] A. Chenel, E. Mangaud, Y. Justum, D. Talbi, M.-C. Bacchus-Montabonel, M. Desouter-Lecomte, Journal of Physics B: Atomic, Molecular and Optical Physics 43 (2010) 245701.

[31] M. Labuda, J. González-Vázquez, F. Martín, L. González, Chemical Physics 400 (2012) 165.

[32] R. Linguerri, M. Hochlaf, M.-C. Bacchus-Montabonel, M. Desouter-Lecomte, Phys. Chem. Chem. Phys. 15 (2013) 824.

[33] J. Suarez, S. Farantos, S. Stamatiadis, L. Lathouwers, Computer Physics Communications 180 (2009) 2025.

[34] J. Suárez, L. Méndez, I. Rabadán, The Journal of Physical Chemistry Letters 6 (2015) 72.

[35] X. Urbain, N. de Ruette, V. M. Andrianarijaona, M. F. Martin, L. F. Menchero, L. F. Errea, L. Méndez, I. Rabadán, B. Pons, Phys. Rev. Lett. 111 (2013) 203201.

[36] R. Guantes, S. C. Farantos, J. Chem. Phys. 111 (1999) 10827.

[37] D. Dundas, J. F. McCann, J. S. Parker, K. T. Taylor, J. Phys. B: At. Mol. Opt. Phys. 33 (2000) 3261.

[38] J. C. Phillips, L. Kleinman, Phys. Rev. 116 (1959) 287.

[39] P. M. M. Gabás, L. F. Errea, L. Méndez, I. Rabadán, Phys. Rev. A 85 (2012) 012702.

[40] C. Illescas, A. Riera, Phys. Rev. Lett. 80 (1998) 3029.

[41] C. Illescas, B. Pons, A. Riera, Phys. Rev. A 63 (2001) 062722.